EXERGETIC ANALYSIS OF AN AIRCRAFT TURBOJET ENGINE WITH AN AFTERBURNER

by

Mehdi Aliehyaei EHYAEI[a]*, Abdolhasan ANJIRIDEZFULI[b], and Mark A. ROSEN[c]

[a] Islamic Azad University, Pardis Branch, Tehran, Iran
[b]Islamic Azad University, Dezful Branch, Dezful City, Khuzestan, Iran
[c]Faculty of Engineering and Applied Science, University of Ontario Institute of Technology, Oshawa, Ont., Canada

Original scientific paper
DOI: 10.2298/TSCI110911043E

An exergy analysis is reported of a J85-GE-21 turbojet engine and its components for two altitudes: sea level and 11,000 meters. The turbojet engine with afterburning operates on the Brayton cycle and includes six main parts: diffuser, compressor, combustion chamber, turbine, afterburner, and nozzle. Aircraft data are utilized in the analysis with simulation data. The highest component exergy efficiency at sea level is observed to be for the compressor, at 96.7%, followed by the nozzle and turbine with exergy efficiencies of 93.7 and 92.3%, respectively. At both considered heights, reducing of engine intake air speed leads to a reduction in the exergy efficiencies of all engine components and overall engine. The exergy efficiency of the turbojet engine is found to decrease by 0.45% for every 1 °C increase in inlet air temperature.

Key words: *turbojet, afterburner, exergy, entropy generation, efficiency*

Introduction

Engines are installed on aircraft for propulsion. Exhaust gases from aircraft engines exit at the rear of the engine nozzle, causing the aircraft to move forward and air to pass over the aircraft wings. This air motion creates lift. Most modern aircraft use gas turbine engines to produce the required thrust force. Such engines are relatively light and compact and have a high power to weight ratios. Aircraft gas turbines operate in an open cycle based on the Brayton cycle. Actual jet cycles are not ideal due to thermodynamic losses. The gases in the jet cycle are expanded in the gas turbine to the pressure that allows generation of the power needed by the compressor, generator, hydraulic pump, and other work-consuming devices. Other gas turbine-based aerospace engines exist beyond the turbojet, including turbofan and turboshaft engines, but only turbojets are considered here. Production of jet aircraft began in 1945, and the technology has advanced significantly since then. Efforts to increase power and reduce noise and fuel consumption have led to improvements in turbojet and turbofan engines [1]. Nearly 16,800 jet aircraft were operating globally in 2007, and this number is expected to increase to 35,300 by 2024 [2]. Due to decreasing world oil reserves, increasing oil prices and increasing environmental concerns, efforts have increased to improve system efficiency. Exergy analysis is a practical and useful tool for such activities, with many engineers and scientists suggesting that exergy analysis is a highly effective method for evaluating and enhancing thermodynamic performance, and superior to energy analysis [3].

* Corresponding author; e-mail: aliehyaei@yahoo.com

Many researchers have investigated aircraft engines and propulsion systems with exergy analysis [4-12]. Rosen and Etele [13, 14] examine the importance of defining a reference environment that varies with altitude and apply that work to a turbojet engine. Gaggioli and Paulus [15] propose a method to account for the exergy rate associated with thrust and lift forces and develop aircraft exergy flow diagrams. Bejan and Siems [16] address the optimization of the cruise velocity and of the heat exchange processes on board an aircraft while Rancruel and Von Spakovsky [17] investigate engine configuration optimization methods. Hunt *et al*. [18, 19], and Riggins *et al*. [20] discuss methodologies for accounting for vehicle wake effects, and Moorhouse and Hoke [21] apply exergy methods to the analysis of the inlet performance. More recently, exergy analysis has been applied to an advanced hypersonic vehicle, with two main scopes: (1) to enhance the exergy approach to the design and optimization of aerospace propulsion systems, through the use of exergy flow diagram that provides aircraft engineers and system designers with insights into avoidable and unavoidable systemic losses, and (2) to explore the limits and merits of fuelling options for a scramjet-powered aircraft [22]. Turgut *et al.* [23] perform an exergoeconomic analysis of an aircraft turbofan engine utilising kerosene as fuel. They develop several parameters (thrust cost rate, cost of exergy destruction, relative cost difference, and exergoeconomic cost) and calculate the thrust cost rate to be 304.35 ($/h kN) and 138.96 ($/h kN) for hot and cold thrust, respectively. Turgut *et al.* [24] apply exergy analysis to a General Electric CF6-80 turbofan engine using sea-level data, and find the units with the greatest irreversibilities in the system to be the fan and the core engine exhaust, which exhibit exergy loss rates of 47.3 MW and 35.9 MW, respectively, and the combustion chamber, which has an exergy destruction rate of 31.5 MW. Previous studies have not examined turbojets with afterburning and have not focused on the variations of the results with altitude. Such information is needed and addressing these needs is the focus of this paper. The main objective is to perform an exergy analysis of a J85-GE-21 turbojet engine and its components, for two altitudes: sea level and 11,000 meters. Entropy generation and exergy efficiency relations are derived for each turbojet engine component and the overall system. The effects are studied of jet velocity and inter air temperature, on entropy generation and exergy efficiency, with the aid of a simulation program developed for this study.

System modeling and analysis

The J85-GE-21 turbojet engine is designed for F-5 fighter aircraft models F and E by General Electric in the US and now is used on this aircraft. A J85-GE-21 turbojet engine is shown in fig. 1, where the main parts are: diffuser, compressor, combustion chamber, turbine, afterburner, and nozzle.

The turbojet has an axial compressor with nine stages, each having a 1.2 compression ratio. The average compression ratio of compressor is 9. The combustion chamber is of an annular type, and has 12 fuel injectors which spray liquid fuel (JET A-1) into the combustion chamber at high pressure. The turbine has two stages and produces the mechanical power needed by the compressor, hydraulic pump, and generator. Twenty fuel injectors spray liquid fuel into the afterburner, where it reacts with all the oxygen in the turbine exhaust gas in to order produce more power and propulsive force. Approximately 15% of the air exiting the diffuser passes around engine for cooling purposes, and is called dead air. The remaining air enters the compressor (40% of the air exiting the compressor goes around combustion chamber and afterburner to keep the flame in the center of these devices). Exhaust gas from turbojet engine is expanded to medium pressure by the nozzle Northrop [25]. Figure 2 shows a schematic diagram of the turbojet engine analyzed.

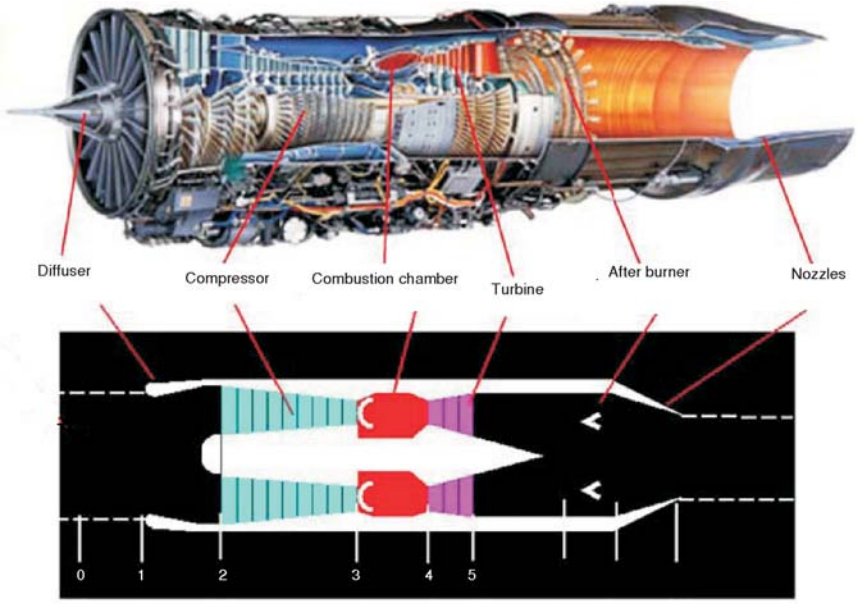

Figure 1. Turbojet engine; used by permission of NASA (see website: www.Nasa.gov)

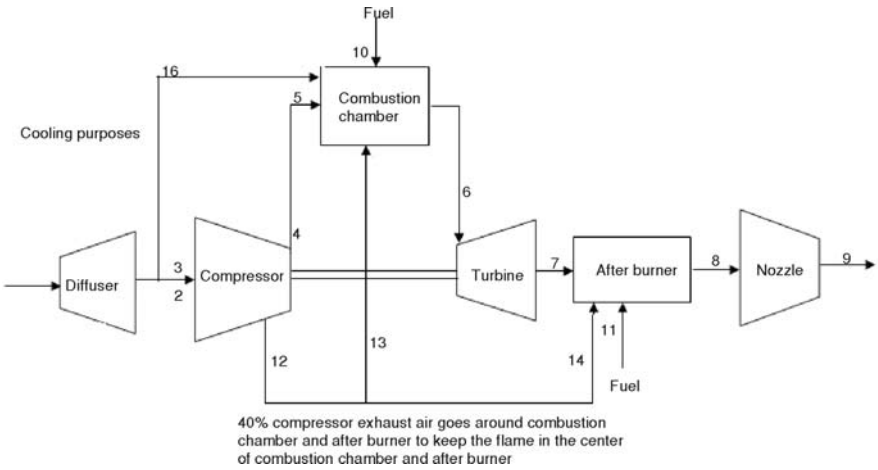

Figure 2. Schematic diagram of turbojet engine

The entry conditions of the diffuser (T_1, P_1, V_1) are known, and the following equations are used to obtain the outlet conditions. Note that outlet diffuser temperature is measured by a sensor installed at the end of diffuser to determine amount of fuel entering the combustion chamber and burning by the engine. The relevant basic equations are as follows:

$$h_0 = h + \frac{V^2}{2} \quad (1), \quad h = u + Pv \quad (2), \quad \eta_D = \frac{h_{02s} - h_1}{h_{01} - h_1} \quad (3)$$

where h_0 [Jkg^{-1}] is the denotes inlet diffuser specific stagnation enthalpy, h [Jkg^{-1}] – the specific enthalpy, V [ms^{-1}] – the velocity, u [Jkg^{-1}] – the specific internal energy, P [Pa] – the pressure, v [m^{3}kg^{-1}] – the specific volume, η_D [Jkg^{-1}] – the diffuser efficiency, h_{0s} [Jkg^{-1}] – the outlet specific stagnation enthalpy for an isentropic process, and h_1 [Jkg^{-1}] – the inlet diffuser specific enthalpy. With the above relations, following equations can be written for the diffuser:

$$h_{01} = h_{02}, \ (4), \qquad V_2 = 0 \ (5), \qquad u_1 + P_1 v_1 + \frac{V_1^2}{2} = u_2 + P_2 v_2 + \frac{V_2^2}{2} \ (6)$$

where h_{01}, and h_{02} [Jkg^{-1}] are the diffuser inlet and outlet specific stagnation enthalpies, u_1 and u_2 [Jkg^{-1}] – the diffuser inlet and outlet specific internal energies, P_1 and P_2 [Pa] – the diffuser inlet and outlet pressures, V_1 [ms^{-1}] – the aircraft velocity, V_2 [ms^{-1}] – the outlet diffuser air speed, and v_1 and v_2 [m^{3}kg^{-1}] – the diffuser inlet and outlet specific volumes . With these equations, the diffuser outlet pressure and temperature can be obtained iteratively. The outlet compressor pressure is obtained with the following equation:

$$P_4 = r_c P_3 \tag{7}$$

where P_4 and P_3 [Pa] are the compressor outlet and inlet pressures, and r_c is the compressor pressure ratio. Also, the outlet compressor temperature is obtained with the following expressions:

$$\mathrm{d}p = T\mathrm{d}s + v\mathrm{d}P \ (8), \qquad \mathrm{d}h_s = v\mathrm{d}P \ (9), \qquad \eta_C = \frac{\mathrm{d}h_s}{\mathrm{d}h} \ (10)$$

Here, dh, [Jkg^{-1}] ds [Jkg^{-1}K^{-1}], and dP [Pa] are the specific enthalpy, specific entropy and pressure variations in the compression process, respectively, T [K] – the average temperature in the compression process, dh_s [Jkg^{-1}] – the specific enthalpy variation for isentropic compression, and η_C – the compressor polytropic efficiency. With the ideal gas assumption and eqs. 8 through 10, the following equation can be developed for the outlet temperature:

$$\overline{C}_P \frac{\mathrm{d}T}{T} = \frac{R}{\eta_C} \frac{\mathrm{d}P}{P} \tag{11}$$

Here, $\overline{C}_P$ [Jkg^{-1}K^{-1}] – the specific heat at constant pressure, which is evaluated at a mean temperature, and R [Jkg^{-1}K^{-1}] – the gas constant. With the specific heat at constant pressure as a function of temperature and the compressor pressure ratio, the compressor outlet temperature can be obtained for gas mixtures by integration of above equation. The integral form of above equation is:

$$\int_{T_3}^{T_4} \overline{C}_P \frac{\mathrm{d}T}{T} = \int_{P_3}^{P_4} \frac{R}{\eta_C} \frac{\mathrm{d}P}{P} = \frac{R}{\eta_C} \int_{P_3}^{P_4} \frac{\mathrm{d}P}{P} \tag{12}$$

Here, T_3 and T_4 [K] are inlet and outlet compressor temperature and P_3 and P_4 [Pa] are inlet and outlet compressor pressure. The compressor power input W_C is calculated as:

$$\dot{W}_C = \dot{m}_a (h_4 - h_3) - 0.4\dot{m}_a h_{12} \tag{13}$$

Here, $\dot{m}_a$ [kgs^{-1}] is air mass flow rate and h_3 and h_4 and h_{12} [Jkg^{-1}] are inlet and outlet specific enthalpies of the compressor. Kerosene is a fuel currently used in aviation. This fuel can have variable functional applications by modification of some of its properties. Two types of kerosene are Jet A and Jet A-1 [26, 27]. Depending on the type of ball bearings, roll bearings, sealing, and packing of selected engines, Jet A-1 or JP4 is normally used [25]. According to fig. 2, there are two components in which combustion occurs. Combustion relations based on reactant and product mass balances are [28]:

– combustion chamber:

$$0.0024C_{12}H_{23} + 0.4944(0.7748N_2 + 0.2059O_2 + 0.0003CO_2 + \\ + 0.019H_2O) \rightarrow 0.02889CO_2 + 0.03694H_2O + 0.05928O_2 + 0.38306N_2 \quad (14)$$

– afterburner:

$$0.0073C_{12}H_{23} + 1.189521(0.762236N_2 + 0.152502O_2 + 0.034138CO_2 + \\ + 0.151124H_2O) \rightarrow 0.1228CO_2 + 0.26371H_2O + 0.072562O_2 + 0.9064N_2 \quad (15)$$

The energy balance for a combustion process can be written as:

$$\sum \dot{m}_r [\mathring{h}_f + (h - h_0)]_p = \eta_{cc} \sum \dot{m}_p [\mathring{h}_f + (h - h_0)]_r \quad (16)$$

where $\mathring{h}_f$ [Jkg^{-1}] is the specific enthalpy of formation, h_0 [Jkg^{-1}] – the specific enthalpy at the reference condition, η_{cc} – the combustion energy efficiency, and the subscripts r and p denote reactants and products, respectively. The combustion temperature can be calculated with eqs. (14) to (16). The pressure in the combustion chamber can be determined as:

$$P_6 = P_5 \frac{n_6}{n_5} \frac{T_6}{T_5} \quad (17)$$

where P_5 and P_6 [Pa] are the inlet and outlet pressures of the combustion chamber, T_5 and T_6 [K] – the inlet and outlet temperatures, and n_6 and n_5 are the inlet and outlet number of moles. Similarly, the pressure in the afterburner can be expressed as:

$$P_8 = P_7 \frac{n_8}{n_7} \frac{T_8}{T_7} \quad (18)$$

where P_7 and P_8 are the inlet and outlet pressures of the afterburner, T_7 and T_8 are the inlet and outlet temperatures, and n_7 and n_8 are the inlet and outlet number of moles. The turbine outlet pressure can be expressed as:

$$P_7 = r_T P_6 \quad (19)$$

where P_7 and P_6 [Pa] are the turbine outlet and inlet pressures, and r_T – the turbine pressure ratio. The turbine outlet temperature can be obtained by the equation:

$$\int_{T_6}^{T_7} \overline{C}_P \frac{dT}{T} = \int_{P_6}^{P_7} \frac{R}{\eta_T} \frac{dP}{P} = \frac{R}{\eta_T} \int_{P_6}^{P_7} \frac{dP}{P} \quad (20)$$

here, T_6 and T_7 are the inlet and outlet turbine temperatures, P_6 and P_7 are inlet and outlet turbine pressures, and η_T – the turbine polytropic efficiency. The turbine power production $\dot{W}_T$ can be expressed as:

$$\dot{W}_T = (\dot{m}_a + \dot{m}_f)(h_6 - h_7) \quad (21)$$

where $\dot{m}_a$ is the air mass flow rate [kgs^{-1}], $\dot{m}_f$ [kgs^{-1}] – the fuel mass flow rate, and h_6 and h_7 [Jkg^{-1}] are the inlet and outlet specific enthalpies of the turbine.The nozzle outlet temperature can be determined using the equations:

$$h_{08} = h_{09} \quad (22), \qquad V_8 = 0 \quad (23), \qquad u_8 + P_8 v_8 \frac{V_8^2}{2} = u_9 P_9 v_9 + \frac{V_9^2}{2} \quad (24)$$

Here, h_{08}, and h_{09} [Jkg^{-1}] are the inlet and outlet nozzle specific stagnation enthalpies, u_8, and u_9 [Jkg^{-1}] – the inlet and outlet nozzle specific internal energies, P_8 and P_9 [Pa] – the inlet and outlet nozzle pressures, V_8 [ms^{-1}] – the inlet nozzle velocity, V_9 [ms^{-1}] – the outlet diffuser air speed, and v_8 and v_9 [m^{3}kg^{-1}] are the nozzle inlet and outlet specific volumes.

Exergy analysis

In the absence of nuclear, magnetic, electric, and surface tension effects, exergy can be divided into four distinct components: physical, chemical, kinetic, and potential [3, 28, 29]:

$$e_{\mathrm{t}} = e_{\mathrm{kn}} + e_{\mathrm{pt}} + e_{\mathrm{ph}} + e_{\mathrm{ch}} \tag{25}$$

where e_{t}, e_{kn}, e_{pt}, e_{ph}, and e_{ch} [Jkg^{-1}] are the total, kinetic, potential, physical, and chemical specific exergies. Specific kinetic and potential exergies can be expressed as:

$$e_{\mathrm{kn}} = \frac{V^2}{2} \quad (26), \qquad e_{\mathrm{pt}} = gh \quad (27)$$

where g [ms^{-2}] is the gravitational acceleration and h [m] – the height. Specific physical and chemical exergies can be written as:

$$e_{\mathrm{ph}} = (h - h_0) - T_0 (s - s_0) \quad (28), \qquad e_{\mathrm{ch}} = \sum_i x_i e_{ch,i} + RT_0 \sum x_i Lnx_i \quad (29)$$

where h [Jkg^{-1}] denotes the specific enthalpy, h_0 [Jkg^{-1}] – the specific enthalpy at the reference condition, s [Jkg^{-1}] – the specific entropy, s_0 [Jkg^{-1}K^{-1}] – the specific entropy at the reference condition, T_0 [K] – the reference temperature, x_{i} – the gas mole fraction, and e_{chi} – specific chemical exergy. Exergy rates [W] can be determined with the equations:

$$\dot{E}_{\mathrm{kn}} = \dot{m} e_{\mathrm{kn}} \quad (30), \qquad \dot{E}_{\mathrm{pt}} = \dot{m} e_{\mathrm{pt}} \quad (31), \qquad \dot{E}_{\mathrm{ph}} = \dot{m} e_{\mathrm{ph}} \quad (32), \qquad \dot{E}_{\mathrm{ch}} = \dot{m} e_{\mathrm{ch}} \quad (33)$$

where $\dot{E}_{\mathrm{kn}}, \dot{E}_{\mathrm{pt}}, E_{\mathrm{ph}},$ and $\dot{E}_{\mathrm{ch}}$ are the kinetic, potential, physical, respectively, and chemical exergy rates $\dot{m}$ and is the mass flow rate.

Since the diffuser is used to increase pressure and reduce velocity and involves no power interaction, the diffuser exergy efficiency can be expressed as:

$$\Psi_{\mathrm{Diffuser}} = \frac{\dot{E}_2}{\dot{E}_1} \tag{34}$$

where Ψ denotes the exergy efficiency, $\dot{E}_2$, and $\dot{E}_1$ [W] are outlet and inlet diffuser exergy rates. The compressor exergy efficiency is calculated as:

$$\Psi_{\mathrm{Compressor}} = \frac{\dot{E}_{12} + \dot{E}_4 - \dot{E}_3}{\dot{W}_{\mathrm{C}}} \tag{35}$$

where $\dot{E}_4, \dot{E}_3,$ and $\dot{E}_{12}$ [W] are the outlet and inlet compressor exergy rates. The combustion chamber exergy efficiency is expressible as:

$$\Psi_{\mathrm{Combustion\ chamber}} = \frac{\dot{E}_6}{\dot{E}_{13} + \dot{E}_5 + \dot{E}_{10}} \tag{36}$$

where $\dot{E}_6$ [W] is the outlet combustion chamber exergy rate, $\dot{E}_5$ [W] – the air inlet combustion chamber exergy rate, $\dot{E}_{10}$ [W] – the fuel exergy consumption rate in the combustion chamber, and $\dot{E}_{13}$[W] – the air exergy consumption rate in the combustion chamber. The turbine exergy efficiency can be written as:

$$\Psi_{\mathrm{Turbine}} = \frac{\dot{W}_t}{\dot{E}_6 - \dot{E}_7} \tag{37}$$

where $\dot{E}_7$ [W] is the outlet turbine exergy rate. The afterburner exergy efficiency can be expressed as:

$$\Psi_{\mathrm{Afterburner}} = \frac{\dot{E}_8}{\dot{E}_{14} + \dot{E}_{11} + \dot{E}_7} \tag{38}$$

where $\dot{E}_8$ [W] is the outlet afterburner chamber exergy rate, $\dot{E}_{11}$[W] – the fuel use exergy rate in the afterburner, and $\dot{E}_{14}$[W] – the air use exergy rate in the afterburner. The nozzle exergy efficiency is determined as:

$$\Psi_{\text{Nozzle}} = \frac{\dot{E}_9}{\dot{E}_8} \tag{39}$$

where $\dot{E}_9$ [W] is the outlet nozzle exergy rate.The overall turbojet exergy efficiency can be written as:

$$\Psi = \frac{\dot{E}_9}{\dot{E}_1 + \dot{E}_{10} + \dot{E}_{11}} \tag{40}$$

The entropy generation rates in the diffuser, compressor, combustion chamber, turbine, afterburner, and nozzle, can be expressed as:

$$\dot{S}_{\text{gen, diffuser}} = \frac{1}{T_o}(\dot{E}_2 - \dot{E}_1) \tag{41}$$

$$\dot{S}_{\text{gen, compressor}} = \frac{1}{T_o}[\dot{E}_{12} + \dot{E}_4 - \dot{E}_3 - (-\dot{W}_c)] \tag{42}$$

$$\dot{S}_{\text{gen, compressor chamber}} = \frac{1}{T_o}(\dot{E}_{13} + \dot{E}_{10} + \dot{E}_5 - \dot{E}_6) \tag{43}$$

$$\dot{S}_{\text{gen, turbine}} = \frac{1}{T_o}(\dot{E}_6 - \dot{E}_7 - \dot{W}_t) \tag{44}$$

$$\dot{S}_{\text{gen, afterburner}} = \frac{1}{T_o}(\dot{E}_7 + \dot{E}_{14} + \dot{E}_{11} - \dot{E}_8) \tag{45}$$

$$\dot{S}_{\text{gen, nozzle}} = \frac{1}{T_o}(\dot{E}_8 - \dot{E}_9) \tag{46}$$

where T_o is the reference environment temperature, which is fixed here at 298.15 K.

Results and discussion

Temperatures, pressures, mass flow rates, kinetic, physical and chemical exergy rates for various parts of engine at sea level and 200 m/s aircraft velocity are shown in tab. 1.

Exergy efficiencies and entropy generation rates for the components of the engine at sea level and 200 m/s speed are shown in figs. 3 and 4, respectively. The highest component exergy

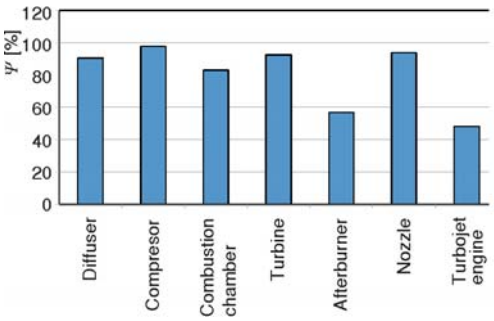

Figure 3. Exergy efficiencies for turbojet engine and its components at sea level and 200 m/s speed

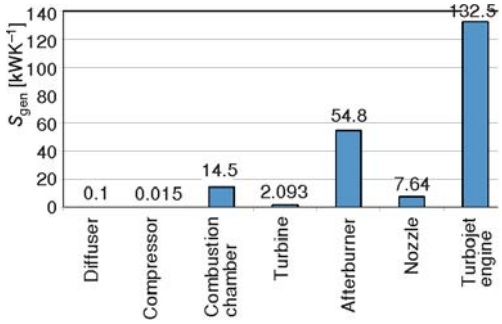

Figure 4. Entropy generation rates for turbojet engine and its components at sea level and 200 m/s speed

Table 1. Thermodynamic parameters for flows in J85GE-21 turbojet engine at sea level and 200 m/s speed

Flow No.	Flow	Temperature [K]	Pressure [kPa]	Mass flow rate [kgs^{-1}]	Physical exergy rate [kW]	Chemical exergy rate [kW]	Kinetic exergy rate [kW]	Total exergy rate [kW]
1	Diffuser inlet	298.1	101.3	28.4	0	0	568.2	568.2
2	Diffuser outlet	318.1	124.2	28.4	514.6	0	0	514.6
3	Compressor inlet	318.1	124.2	24.1	437.4	0	0	437.4
4	Compressor outlet	625.7	1118.2	24.1	7679.5	0	0	7679.5
5	Combustion chamber inlet	625.7	1118.2	14.5	4607.7	0	0	4607.7
6	Turbine inlet	1709.6	2138.8	14.9	18409.2	0	0	18409.2
7	Afterburner inlet	1184	534.7	14.9	10297.4	0	0	10297.4
8	Afterburner outlet	2933.5	1263.8	19	36170.4	0	0	36170.4
9	Nozzle outlet	2866.1	101.3	19	32781.3	0	1111.1	33892.4
10	Combustion chamber fuel input	353	2757	0.4	0	18282.3	0	18282.3
11	Afterburner fuel input	353	1103.1	218.1	0	55688	0	55688
12	Compressor cooling output	625.7	1118.2	9.6	3071.8	0	0	3071.8
13	Combustion chamber cooling air input	625.7	1118.2	5.8	1843.1	0	0	1843.1
14	Afterburner cooling air input	625.7	1118.2	3.8	1228.7	0	0	1228.7

efficiency is exhibited by the compressor at 96.7%. The next highest exergy efficiencies are for the nozzle (93.7%) and turbine (92.3%). The lowest exergy efficiencies are for the afterburner (54.8%), followed by the combustion chamber (80.4%). The low fuel efficiency of the afterburner compared to the combustion chamber results in it burning almost three times the fuel of the combustion chamber, in order to increase the thrust force by about one third. The entropy production rates also help identify the components with the highest irreversibilities. The greatest entropy production rate in the engine is observed for the afterburner, followed by the combustion chamber. Hence, the combustion processes in the aircraft engine are highly irreversible. The nozzle, due to the rapid changes in cross-sectional area has in the third highest entropy production rates.

To determine the effect of aircraft engine velocity on entropy production rate and exergy efficiency, the engine velocity is reduced from 200 m/s to 100 m/s and the results re-determined (see tab. 2). For this case, the exergy efficiencies and entropy generation rates are shown in figs.

Table 2. Thermodynamic parameters for flows in J85GE-21 turbojet engine at sea level and 100 m/s speed

Flow No.	Flow	Temperature [K]	Pressure [kPa]	Mass flow rate [kgs^{-1}]	Physical exergy rate [kW]	Chemical exergy rate [kW]	Kinetic exergy rate [kW]	Total exergy rate [kW]
1	Diffuser inlet	298.1	101.3	14.2	0	0	71	71
2	Diffuser outlet	303	106.7	14.2	64	0	0	64
3	Compressor inlet	303	160.7	12.1	54.4	0	0	54.4
4	Compressor outlet	596.3	960.5	12.1	3483.6	0	0	3483.6
5	Combustion chamber inlet	596.3	960.5	7.2	2090.1	0	0	2090.1
6	Turbine inlet	1684.6	1899.4	7.6	9500.8	0	0	9500.8
7	Afterburner inlet	1166.7	474.9	7.6	5082.9	0	0	5082.9
8	Afterburner outlet	29.48.6	1144.9	9.9	19098.6	0	0	19098.6
9	Nozzle outlet	2880.2	101.3	9.9	17408.6	0	592	18000.6
10	Combustion chamber fuel input	353	2757	0.4	0	18282.3	0	18282.3
11	Afterburner fuel input	353	1103.1	1.2	0	55687.9	0	55687.9
12	Compressor cooling output	596.3	960.5	4.8	2090	0	0	2090
13	Combustion chamber cooling air input	596.3	960.5	2.9	1254	0	0	1254
14	Afterburner cooling air input	596.3	960.5	1.92	836	0	0	836

5 and 6. The exergy efficiencies the overall engine of all it components decrease as the engine velocity decreases due to the reduction air mass flow rate.

To evaluate the variation of the performance of aircraft engine and its components with altitude, the performance parameters considered earlier are evaluated for an altitude of 11,000 m, which is a typical altitude at which a majority of aircraft flight time is spent. The temperature and pressure at high altitudes are much different than at sea level. For instance, these parameters

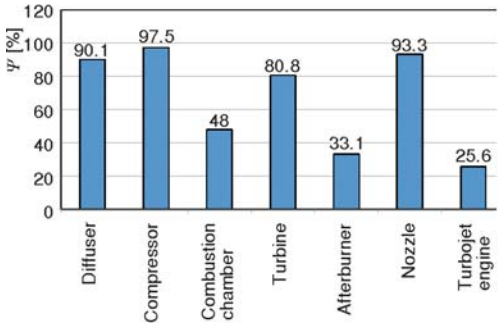

Figure 5. Exergy efficiencies for turbojet engine and its components at sea level and 100 m/s speed

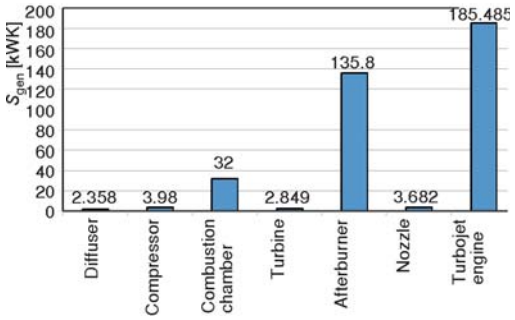

Figure 6. Entropy generation rates for turbojet engine and its components at sea level and 100 m/s speed

were measured as 220 K and 4.23 kPa, respectively, by the meteorological office on February 17, 2010, at 10 a. m. at an altitude 11,000 m. The temperatures, pressures, mass flow rates, and

Table 3. Thermodynamic parameters for flows in J85GE – 21 turbojet engine at 11,000 m altitude and 200 m/s speed

Flow No.	Flow	Temperature [K]	Pressure [kPa]	Mass flow rate [kgs^{-1}]	Physical exergy rate [kW]	Chemical exergy rate [kW]	Kinetic exergy rate [kW]	Total exergy rate [kW]
1	Diffuser inlet	220.15	23.4	8.9	0	0	177.8	177.8
2	Diffuser outlet	240	30.8	8.9	161.3	0	0	161.3
3	Compressor inlet	240	3.8	7.6	137.1	0	0	137.1
4	Compressor outlet	472.23	276.9	7.6	1830.1	0	0	1830.1
5	Combustion chamber inlet	472.23	276.9	4.5	1098	0	0	1098
6	Turbine inlet	1586.6	651.2	4.7	6135.3	0	0	6135.3
7	Afterburner inlet	1098.8	162.8	4.7	3356.8	0	0	3356.8
8	Afterburner outlet	2823.5	399.1	5.8	12423.2	0	0	12423.2
9	Nozzle outlet	2777.7	23.4	5.8	11465.9	0	256.7	11722.6
10	Combustion chamber fuel input	320	2757	0.13	0	5745.2	0	5745.2
11	Afterburner fuel input	320	1103.2	0.38	0	17500	0	17500
12	Compressor cooling output	472.23	276.9	3.04	1098	0	0	1098
13	Combustion chamber cooling air input	472.23	276.9	1.8	658.8	0	0	658.8
14	Afterburner cooling air input	472.23	276.9	1.22	439.2	0	0	439.2

Table 4. Thermodynamic parameters for flows in J85GE-21 turbojet engine at 11,000 m altitude and 100 m/s speed

Flow No.	Flow	Temperature [K]	Pressure [kPa]	Mass flow rate [kgs^{-1}]	Physical exergy rate [kW]	Chemical exergy rate [kW]	Kinetic exergy rate [kW]	Total exergy rate [kW]
1	Diffuser inlet	220.1	23.4	4.4	0	0	22.2	22.2
2	Diffuser outlet	225.1	25.1	4.4	20	0	0	20
3	Compressor inlet	225.1	25.1	3.8	17	0	0	17
4	Compressor outlet	442.9	226	3.8	806.3	0	0	806.3
5	Combustion chamber inlet	442.9	226	2.3	483.8	0	0	483.8
6	Turbine inlet	1562.6	558.1	2.4	3367.2	0	0	3367.2
7	Afterburner inlet	1082.2	139.5	2.4	1659.9	0	0	1659.9
8	Afterburner outlet	2828.85	347.9	3.1	6588.2	0	0	6588.2
9	Nozzle outlet	2782.6	23.4	3.1	6106.9	0	136.8	6243.7
10	Combustion chamber fuel input	320	2757	0.13	0	5745.2	0	5745.2
11	Afterburner fuel input	320	1103.1	0.38	0	17499.9	0	17499.9
12	Compressor cooling output	442.9	226	2.28	483.78	0	0	493.8
13	Combustion chamber cooling air input	442.9	226	1.4	290.3	0	0	296.3
14	Afterburner cooling air input	442.9	226	0.88	193.5	0	0	197.5

kinetic, physical, and chemical exergy rates for various components of the engine at altitude of 11,000 m and a 200 m/s aircraft velocity are shown in tab. 3. Exergy efficiencies and entropy generation rates the engine and its components at an altitude of 11,000 m and an engine speed of 200 m/s are shown in figs. 7 and 8. The compressor has the highest exergy efficiency at 95.7%, followed by the diffuser (94.8%) and nozzle (90.5%).

To evaluate the variation of the performance of aircraft engine and its components with aircraft velocity at high altitude, the entropy production rates and exergy efficiencies are evaluated when the engine velocity is reduced from 200 m/s to 100 m/s at an altitude of 11,000 m The results are given in tab. 4. For this case, the exergy efficiencies and entropy generation rates are shown in figs. 9 and 10.

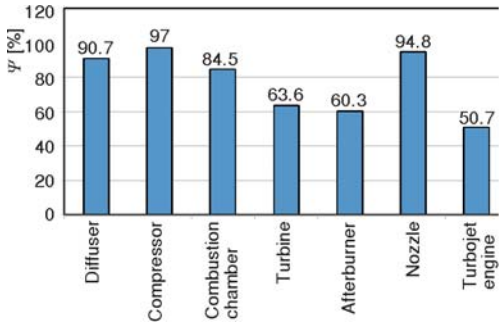

Figure 7. Exergy efficiencies for turbojet engine and its components at 11,000 m altitude and 200 m/s speed

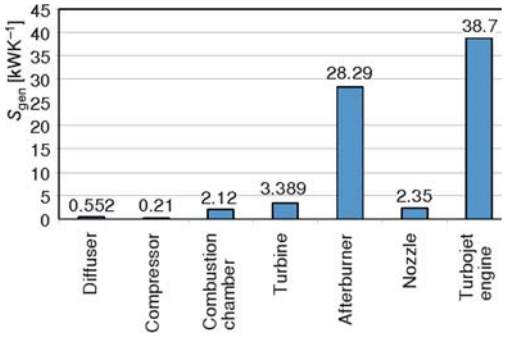

Figure 8. Entropy generation rates for turbojet engine and its components at 11,000 m altitude and 200 m/s speed

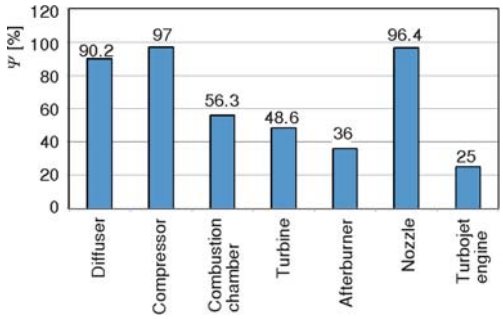

Figure 9. Exergy efficiencies for turbojet engine and its components at 11,000 m and 100 m/s speed

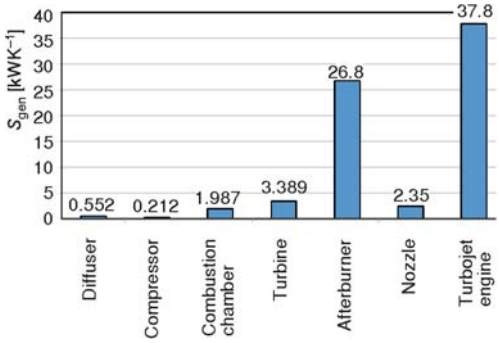

Figure 10. Entropy generation rates for turbojet engine and its components at 11,000 m and 100 m/s speed

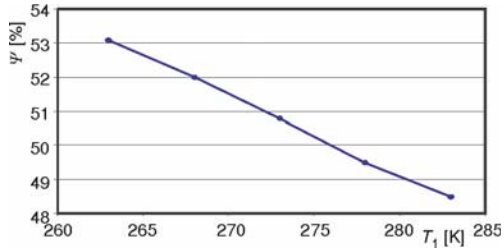

Figure 11. Variation of aircraft exergy efficiency on aircraft engine

The effect of inlet air temperature on exergy efficiency for the aircraft engine is shown in fig. 11. The overall exergy efficiency of the aircraft engine is reduced 0.45% for each centigrade degree increase in inlet air temperature. The cause of this phenomenon is the decrease in air density due to the increase in temperature. This observation suggests that flying in early hours of the day or at night is economic due to the lower ambient temperature.

Conclusions

The exergy analysis of the selected aircraft engine with afterburner operating on kerosene fuel for various altitudes and air speeds reveals useful insights, as does the investigation of the effects of aircraft inlet air temperature on exergy efficiency. The relations are quantified between exergy efficiency and entropy generation for the components of the aircraft engine. The key results and conclusions are:

- The highest component exergy efficiency is observed at sea level for the compressor (96.7%), followed by the nozzle (93.7%), and turbine (92.3%). Similarly, the highest exergy efficiency at an altitude of 11,000 m is exhibited by the compressor (95.7%), followed by the nozzle (94.8%), and the diffuser (90.5%).
- The lowest component exergy efficiency at sea level is observed for the afterburner (54.8%), followed by the combustion chamber (80.4%). Correspondingly, the entropy production rates at sea level indicate that the most irreversible process is the afterburner, followed by the combustion chamber and nozzle.
- Reducing aircraft velocity at sea level reduces the exergy efficiency of the aircraft engine and its components.
- The aircraft engine exergy efficiency is reduced 0.45% per centigrade degree increase in inlet air temperature.

Nomenclature

C_p – specific heat at constant pressure, [Jkg^{-1}]
$\mathrm{d}h$ – specific enthalpy variation in process, [Jkg^{-1}]
$\mathrm{d}h_s$ – specific enthalpy variation in isentropic process, [Jkg^{-1}]
$\dot{E}_{ch}$ – chemical exergy rate, [W]
$\dot{E}_{kn}$ – kinetic exergy rate, [W]
$\dot{E}_{ph}$ – physical exergy rate, [W]
E_{pt} – potential exergy rate, [W]
e_t – specific exergy, [Jkg^{-1}]
g – gravitational acceleration, [ms^{-2}]
h – height of aircraft, [m]
h – specific enthalpy, [Jkg^{-1}]
h_0 – specific enthalpy at reference condition, [Jkg^{-1}]
h_f – specific enthalpy of formation, [Jkg^{-1}]
h_{01} – inlet specific stagnation enthalpy, [Jkg^{-1}]
h_{02} – outlet specific stagnation enthalpy, [Jkg^{-1}]
h_{0S} – outlet specific stagnation enthalpy in isentropic process, [Jkg^{-1}]
$\dot{m}$ – mass flow rate, [kgs^{-1}]
$\dot{m}_a$ – air mass flow rate, [kgs^{-1}]
$\dot{m}_f$ – fuel mass flow rate, [kgs^{-1}]
n – number of moles
P – pressure, [Pa]
R – gas constant, [Jkg^{-1}K^{-1}]
r_c – compressor pressure ratio
r_T – turbine pressure ratio
T – mean temperature in compression process, [K]
T_o – reference environment temperature, [K]
u – specific internal energy, [Jkg^{-1}]
V – velocity, [ms^{-1}]
V_1 – aircraft velocity, [ms^{-1}]
v – specific volume, [m^{3}kg^{-1}]
$\dot{W}_C$ – compressor input power, [W]
$\dot{W}_T$ – turbine output power, [W]

Greek symbols

η_c – compressor polytropic efficiency
η_D – diffuser polytropic efficiency
η_T – turbine polytropic efficiency
Ψ – second law efficiency

Subscripts

ch – chemical
kn – kinetic
p – product
ph – physical
pt – potential
r – reactant
1 – diffuser inlet
2 – diffuser out let
3 – compressor Inlet
4 – compressor outlet
5 – combustion chamber inlet
6 – combustion chamber outlet
7 – afterburner inlet or turbine outlet
8 – afterburner outlet or nozzle inlet
9 – nozzle outlet
10 – combustion chamber inlet
11 – afterburner inlet
12 – compressor cooling air outlet
13 – combustion chamber cooling air inlet
14 – afterburner cooling air inlet

References

[1] Balli, O., *et al*., Exergetic and Exergoeconomic Analysis of an Aircraft Jet Engine (AJE), *International Journal of Exergy, 5* (2004), 6, pp. 567-581
[2] Karakoc, H., *et al*., Exergetic Analysis of an Aircraft Turbofan Engine, *Proceedings,* Summer Course on Exergy and its Applications, Anadolu University, Eskisehir, Turkey, 2006, pp. 14-16

[3] Dincer, I., Rosen, M. A., *Exergy: Energy, Environment, and Sustainable Development*, Elsevier, Oxford, 2007
[4] Riggins, D., McClinton, C., Thrust Modeling for Hypersonic Engines, AIAA paper 95-6081, 1995
[5] Riggins, D. W., High-Speed Engine/Component Performance Assessment Using Exergy and Thrust-Based Methods, report NASA-CR-198271, National Aeronautics and Space Administration, Langley Research Center, Hampton, Va., USA, 1996a
[6] Riggins, D. W., The Evaluation of Performance Losses in Multi-Dimensional Propulsive Flows, AIAA paper 96-0375, 1996b
[7] Riggins, D. W., Brayton Cycle Engine/Component Performance Assessment Using Energy and Thrust-Based Methods, AIAA paper 96-2922, 1996
[8] Riggins, D. W., Evaluation of Performance Loss Methods for High-Speed Engines and Engine Components, *Journal of Propulsion and Power, 13* (1997), 2, pp. 296-304
[9] Riggins, D., The Thermodynamic Continuum of Jet Engine Performance: The Principle of Lost Work Due to Irreversibility in Aerospace System, *International Journal of Thermodynamics, 6* (2003), 3, pp. 107-120
[10] Curran, E. T., The Use of Stream Thrust Concepts for the Approximate Evaluation of Hypersonic Ramjet Engine Performance, US Air Force Aero Propulsion Laboratory, Report AFAPL-TR-73-38, Wright-Patterson Air Force Base, O., USA, 1973
[11] Brilliant, H. M., Analysis of Scramjet Engines Using Exergy Methods, AIAA paper 95-2767, 1995
[12] Horlock, J., Thermodynamic Availability and Propulsion, AIAA paper 99-741, 1999
[13] Rosen, M. A., Etele, J., The Impact of Reference Environment Selection on the Exergy Efficiencies of Aerospace Engines, *ASME Advanced Energy System, 39* (1999), 3, pp. 583-591
[14] Rosen, M. A., Etele, J., Aerospace System and Exergy Analysis: Application and Methodology Development Needs, *International Journal of Exergy, 1* (2004), 4, pp. 411-425
[15] Gaggioli, R. A., Paulus, J. D., The Exergy of Lift, and Aircraft Exergy Flow Diagrams, *International Journal of Thermodynamics, 6* (2003), 4, pp. 149-156
[16] Bejan, A., Siems, D. L., The Need for Exergy Analysis and Thermodynamic Optimization and Aircraft Development, *International Journal of Exergy, 1* (2001), 1, pp. 14-24
[17] Rancruel, D. F., Von Spakovsky, M. R., Decomposition with Thermoeconomic Isolation Applied to the Optimal Synthesis/Design of an Advanced Fighter Aircraft System, *International Journal of Thermodynamics, 6* (2003), 3, pp. 121-129
[18] Hunt, L., *et al*., Wake Integration for Three Dimensional Flow Field Computations, Theoretical Development, *Journal of Aircraft, 36* (1999a), 2, pp. 357-365
[19] Hunt, L., *et al*., Wake Integration for Three Dimensional Flow Field Computations, *Application' Journal of Aircraft, 36* (1999b), 2, pp. 366-373
[20] Riggins, D., *et al*., Methodology for the Performance Analysis of Aerospace Vehicles Using the Laws of Thermodynamics, *Journal of Aircraft, 43* (2006), 4, pp. 953-963
[21] Moorhouse, D. J., Hoke, C. M., Thermal Analysis of Hypersonic Inlet Flow with Exergy-Based Design Methods, *International Journal of Applied Thermodynamics, 5* (2002), 4, pp. 161-168
[22] Amati, V., *et al*., Exergy Analysis of Hypersonic Propulsion Systems: Performance Comparison of Two Different Scramjet Configurations at Cruise Conditions, *Energy: An International Journal, 33* (2008), 2, pp. 116-129
[23] Turgut, E. T., *et al*., Exergoeconomic Analysis of an Aircraft Turbofan Engine, *International Journal of Exergy, 6* (2009), 3, pp. 277-294
[24] Turgut, E. T., *et al.*, Exergy Analysis of a Turbofan Aircraft Engine, *International Journal of Exergy, 6* (2009), 2, pp. 181-199
[25] ***, Northrop Co. Technical Order of Aircraft 1F-5E/F, Report, 1978
[26] Dagaut, B., Cathonnet, P., The Ignition, Oxidation and Combustion of Kerosene: A Review of Experimental and Kinetic Modeling, *Progress in Energy and Combustion Science, 32* (2006), 1, pp. 48-92
[27] Sochet, I., Gillard, P., Flammability of Kerosene in Civil and Military Aviation, *Journal of Loss Prevention in the Process Industries, 5* (2002), 3, pp. 335-345
[28] Bejan, A., *Advanced Engineering Thermodynamics*, John Wiley and Sons, New York, USA, 1998
[29] Bejan, A., *et al.*, *Thermal Design and Optimization*, John Wiley and Sons, New York, USA, 1998

Paper submitted: September 11, 2011
Paper revised: April 13, 2012
Paper accepted: August 24, 2012